

Chapter 1

Varying fundamental constants meet Hubble

Jens Chluba and Luke Hart

Abstract Fundamental physical constants need not be constant, neither spatially nor temporally. – This seeming simple statement has profound implications for a wide range of physical processes and interactions, and can be probed through a number of observations. In this chapter, we highlight how CMB measurements can constrain variations of the fine-structure constant and the electron rest mass during the cosmological recombination era. The sensitivity of the CMB anisotropies to these constants arises because they directly affect the cosmic ionization history and Thomson scattering rate, with a number of subtle atomic physics effects coming together. Recent studies have revealed that variations of the electron rest mass can indeed alleviate the Hubble tension, as we explain here. Future opportunities through measurements of the cosmological recombination radiation are briefly mentioned, highlighting how these could provide an exciting avenue towards uncovering the physical origin of the Hubble tension experimentally.

Jens Chluba (✉)
Jodrell Bank Centre for Astrophysics, Alan Turing Building, University of Manchester, Manchester M13 9PL, United Kingdom
e-mail: jens.chluba@manchester.ac.uk

Luke Hart (✉)
Jodrell Bank Centre for Astrophysics, Alan Turing Building, University of Manchester, Manchester, M13 9PL, United Kingdom
TNEI Services Ltd., Bainbridge House, 88 London Road, Manchester, M1 2PW, United Kingdom
e-mail: luke.hart@tneigroup.com

1.1 Why varying fundamental constants?

The laws of nature depend on fundamental constants (FCs) such as Newton’s constant, G , the speed of light, c , and elementary charge of an electron, e , to name just a few. The values of these constants have been determined experimentally, but generally should emerge directly from the underlying theory. As such, there is no reason to assume that the values of the FCs determined locally simply translate to other parts of the cosmos or to other eras in cosmic history [94, 95, 60]. Studies of fundamental constants and their possible temporal and spatial variations are thus of utmost importance, and could provide a glimpse at physics beyond the standard model, possibly shedding light on the presence of additional scalar fields and their couplings to the standard sector.

Of the many fundamental constants, the fine-structure constant, α_{EM} , and electron rest mass, m_e , are the most interesting to CMB studies [48, 7, 8, 6, 75, 61, 83, 63]. This is because these constants play crucial roles in the way photons and baryons interact. Most importantly, they affect important atomic transition rates, which in turn control the cosmological recombination process and hence the Thomson visibility function (defining the last scattering surface) that is so crucial to the formation of the CMB temperature and polarization anisotropies [92, 66, 43, 42, 58].

Using *Planck* 2013 data, the values of α_{EM} and m_e around recombination were proven to coincide with those obtained in the lab to within $\simeq 0.4\%$ for α_{EM} and $\simeq 1\% - 6\%$ for m_e [68]. These limits are $\simeq 2 - 3$ orders of magnitude weaker than constraints obtained from other ‘local’ measurements [11, 76, 12, 54]; however, the CMB places limits during very different phases in the history of the Universe, centered around the time of last scattering some 380,000 years after the Big Bang, thereby complementing these low-redshift measurements. In addition, CMB measurements can be used to probe spatial variations of the FCs at cosmological distances [89], opening yet another avenue for exploration.

With the *Planck* 2013 results in mind, no significant surprises were expected from the analysis of improved CMB data of the *Planck* 2015 and 2018 releases. However, it turns out that when considering models with varying m_e , the geometric degeneracy becomes significant and can accommodate shifts in the value of the Hubble parameter when multiple probes are combined [36]. The same geometric freedom is not encountered when varying α_{EM} due to the modified dependence of the visibility function on this parameter. This finding has spurred an increased interest in studying VFCs in this context, with scenarios that allow for varying m_e [86, 55, 93, 41] ranking high in model comparisons [82]. Since VFCs can be caused by the presence of scalar fields [9, 62], a natural question is whether the same scalar fields could also be causing effects relating to EDE (see [72, 73]), indicating a ‘two sides of the same coin’ interplay. It will therefore be extremely important to ask how different measurements can be combined to shed light on the physical origin of the Hubble tension.

In this Chapter we explain how α_{EM} and m_e enter the cosmological recombination problem and calculation of the CMB power spectra. We then briefly recap some of the constraints, highlighting important findings, before moving on to a discussion

of their role in the Hubble tension. Modifications to the recombination process also affect the cosmological recombination radiation (CRR) [91, 15], implying that direct insight into the underlying physics could be gained by future measurements of CMB spectral distortions [14]. We highlight how this avenue may even allow distinguishing models of EDE, PMFs and VFCs and possibly identify modifications to the recombination history as the main cause of the tension [38, 59].

1.2 Effects of VFCs on the recombination process

The ionization history of the Universe is one of the crucial theoretical ingredients in the computations of the CMB temperature and polarization anisotropies [92, 66, 42]. The first computations of this transition from the fully-ionized plasma to a neutral medium were carried out in the late 60s, recognizing the important role of Lyman- α transport and the 2s-1s two-photon decay of Hydrogen [97, 65]. These early calculations reached a precision of $\simeq 20\% - 30\%$ in the free electron fraction, $X_e = N_e/N_H$, around the maximum of the Thomson scattering visibility function at redshift $z \simeq 1100$. Here N_e is the free electron number density and N_H denotes the total number density of hydrogen nuclei in the Universe. However, with the advent of precision CMB data from *WMAP* and *Planck* it became important to improve the modeling of the cosmological recombination process [42, 18, 58]. Initially, this led to the development of *Recfast* [84], which reached $\simeq 1\% - 3\%$ precision for Hydrogen and neutral Helium recombination. However, for the analysis of data from *Planck*, this precision was still insufficient, and many detailed atomic physics and radiative transfer effects had to be accounted for [31, 91, 96, 77, 33], leading to changes at the level of several standard deviations in particular for the value of the spectral index of scalar perturbations, n_s [77, 87]. This necessitated the development of the highly-flexible and accurate recombination codes *CosmoRec* [22] and *HyRec* [5], which ensured that for the analysis of *Planck* none of the standard parameters were biased at a significant level [67, 69].

This short recap highlights the crucial role of the recombination history in the computations of the CMB anisotropies using standard Boltzmann solvers such as *CAMB* [57] and *CLASS* [56], and conversely, the impressive precision and sensitivity of the current measurements to subtle modifications in the ionization history. The statements assume standard physics during the recombination era at $z \simeq 10^2 - 10^4$. In particular, it is assumed that the atomic transition rates for Hydrogen and Helium are the same as those inferred in the lab.

From standard textbook atomic physics, it is well-understood how α_{EM} and m_e affect the energy levels and transition probabilities of Hydrogen and Helium [10, 25]. It is immediately clear that varying α_{EM} and m_e inevitably create changes to the cosmological ionization history and hence CMB observables. Most importantly, the energy levels of hydrogen and helium depend on these constants as $E_i \propto \alpha_{EM}^2 m_e$, which directly affects the recombination redshift. In addition, the atomic bound-bound transition rates and photoionization/recombination rates are

altered when varying α_{EM} and m_e . Lastly, the interactions of photons and electrons through Compton and resonance scattering modify the radiative transfer physics, which control the dynamics of recombination [19, 51, 78, 40, 21, 4, 16].

In an effective three-level atom approach [97, 65, 85], the individual dependencies can be summarized as [48, 83, 68, 34]

$$\begin{aligned} \sigma_{\text{T}} &\propto \alpha_{\text{EM}}^2 m_e^{-2} & A_{2\gamma} &\propto \alpha_{\text{EM}}^8 m_e & P_{\text{S}} A_{1\gamma} &\propto \alpha_{\text{EM}}^6 m_e^3 \\ \alpha_{\text{rec}} &\propto \alpha_{\text{EM}}^2 m_e^{-2} & \beta_{\text{phot}} &\propto \alpha_{\text{EM}}^5 m_e & T_{\text{eff}} &\propto \alpha_{\text{EM}}^{-2} m_e^{-1}. \end{aligned} \quad (1.1)$$

Here, σ_{T} denotes the Thomson scattering cross section; $A_{2\gamma}$ is the two-photon decay rate of the second shell; α_{rec} and β_{phot} are the effective recombination and photoionization rates, respectively; T_{eff} is the effective temperature at which α_{rec} and β_{phot} need to be evaluated (see explanation below); $P_{\text{S}} A_{1\gamma}$ denotes the effective dipole transition rate for the main resonances (e.g., Lyman- α), which is reduced by the Sobolev escape probability, $P_{\text{S}} \leq 1$ [90, 85] with respect to the vacuum rate, $A_{1\gamma}$. For a more detailed account of how the transition rates depend on the fundamental constants we refer to `CosmoSpec` [15] and the manual of `HyRec` [5].

The scalings of σ_{T} , $A_{2\gamma}$ and $P_{\text{S}} A_{1\gamma}$ directly follow from their explicit dependence on α_{EM} and m_e . For α_{rec} and β_{phot} , only the renormalisations of the transition rates is reflected, again stemming from their explicit dependencies on α_{EM} and m_e [49]. However, these rates also depend on the ratio of the electron and photon temperatures to the ionization threshold. This leads to an additional dependence on α_{EM} and m_e , which can be captured by evaluating these rates at a rescaled temperature, with a scaling indicated through T_{eff} . Overall, this leads to the effective dependence $\alpha_{\text{rec}} \propto \alpha_{\text{EM}}^{3.44} m_e^{-1.28}$ around hydrogen recombination [15]. The required photoionization rate, β_{phot} , is obtained using the detailed balance relation. Slightly different overall scalings for α_{rec} and β_{phot} were used in [68], but the associated effect on the recombination history were found to be sub-dominant and limited to $z \lesssim 800$ [34].

For neutral helium, non-hydrogenic effects (e.g., fine-structure transitions, singlet-triplet couplings) become relevant [25, 26]. However, the corrections should be sub-dominant and are usually neglected. A detailed discussion of changes to the escape probabilities during helium recombination can be found in [38]. In [34], the changes to helium and hydrogen recombination were furthermore treated separately.

1.2.1 Ionization history modifications due to variation of α_{EM}

Given the above ingredients, one can now answer the question about how various effects propagate to the ionization history. A detailed study that also directly demonstrated the validity of simpler three-level approximations against `CosmoRec` was carried out in [34]. The overall effect of varying α_{EM} is illustrated in Fig. 1.1, assuming a constant variation parametrized as $\alpha_{\text{EM}} = \alpha_{\text{EM},0}(1 + \Delta\alpha/\alpha)$, where $\alpha_{\text{EM},0} = 1/137$ denotes the standard value. Increasing the fine structure constant shifts the moment of recombination toward higher redshifts. This agrees with the

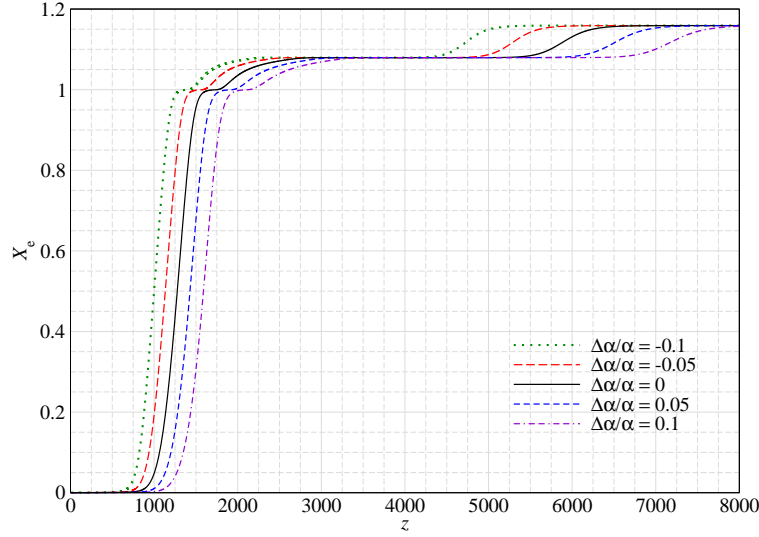


Fig. 1.1: Ionization histories for different values of α_{EM} . The dominant effect is caused by modifications of the ionization threshold, which implies that for increased α_{EM} recombination finishes earlier. The curves were computed using the Recfast++ module of CosmoRec [22]. The figure was taken from [34].

results found earlier in [48, 8, 75] and can intuitively be understood in the following manner: $\Delta\alpha/\alpha > 0$ increases the transition energies between different atomic levels and the continuum. This increases the energy threshold at which recombination occurs, hence increasing the recombination redshift, an effect that is basically captured by an effective temperature rescaling in the evaluation of the photoionization and recombination rates (see below).

The relative changes to the ionization history, $\Delta X_e/X_e$, for the different quantities in Eq. (1.1) are illustrated in Fig. 1.2. We chose a value for $\Delta\alpha/\alpha = 10^{-3}$, which leads to a percent-level effect on X_e . As expected, the biggest effect appears after rescaling the temperature for the evaluation of the photoionization and recombination rates. More explicitly, this can be understood when considering the net recombination rate to the second shell, which can be written as¹

$$\Delta R_{\text{con}} = N_e N_p \alpha_{\text{rec}} - N_2 \beta_{\text{phot}} = \alpha_{\text{rec}} [N_e N_p - g(T_\gamma) N_2],$$

where $g(T_\gamma) \propto T_\gamma^{3/2} e^{-hv_{2c}/kT_\gamma}$ with continuum threshold energy, $E_{2c} = hv_{2c}$. Here, the exponential factor (\leftrightarrow Boltzmann factor) is most important, leading to an exponential effect once we replace $T_\gamma'(z) = T_\gamma(z) \times (\alpha_{\text{EM}}/\alpha_{\text{EM},0})^{-2} (m_e/m_{e,0})^{-1}$.

¹ In full equilibrium, $\Delta R_{\text{con}} = 0$.

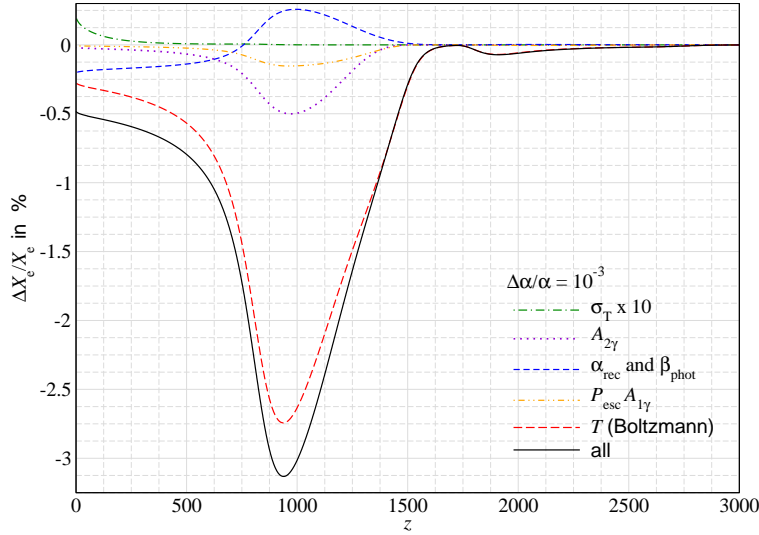


Fig. 1.2: The relative changes in the ionization history for $\Delta\alpha/\alpha = 10^{-3}$ with respect to the standard case caused by different effects. Recfast++ was used for the computations. The rescaling of temperature (\leftrightarrow mainly affecting the Boltzmann factors) yields $\Delta X_e/X_e \simeq -2.7\%$, dominating the total contributions, which peaks with $\simeq -3.1\%$ at $z \simeq 1000$. Note that the modification due to σ_T has been scaled by a factor of ten to make it visible. The figure was taken from [34].

The second largest individual effect is due to the rescaling of the two-photon decay rate, $A_{2\gamma}$. This is expected since α_{EM} appears in a high power, $A_{2\gamma} \propto \alpha_{\text{EM}}^8$, and also because the 2s-1s two-photon channel plays such a crucial role for the recombination dynamics [97, 65, 18], allowing $\simeq 58\%$ of all hydrogen atoms to become neutral through this route [17].

The normalizations of the recombination and photoionization rates (blue/dashed line in Fig. 1.2) give rise to a net delay of $\Delta X_e/X_e \simeq 0.3\%$ at $z \simeq 1000$, which partially cancels the acceleration due to $A_{2\gamma}$. This is due to the stronger scaling of β_{phot} with α_{EM} than α_{rec} . At low redshifts ($z \lesssim 750$), recombination is again accelerated, indicating that a higher fraction of recombination events occurs, as the importance of photoionization ceases. The correction related to the Lyman- α channel is found to be $\simeq 3.3$ times smaller than for the two-photon channel, yielding $\Delta X_e/X_e \simeq -0.15\%$ at $z \simeq 1000$. Finally, the effect of rescaling σ_T are very small and only becomes noticeable at low redshifts. At these redshifts, the matter and radiation temperature begins to depart, giving $T_e < T_\gamma$. For larger α_{EM} , this departure is delayed, such that T_e stays longer close to T_γ . Hotter electrons recombine less efficiently, so that a slight delay of recombination appears (cf., Fig. 1.2).

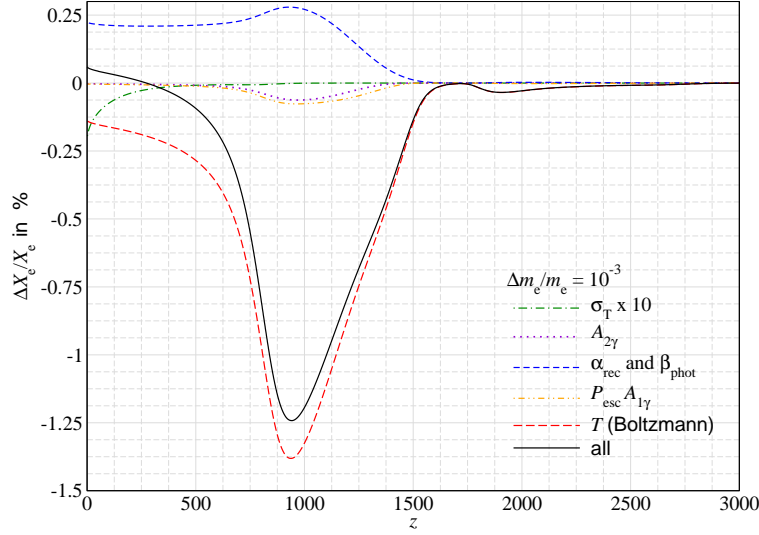


Fig. 1.3: Same as in Fig. 1.2 but for $\Delta m_e/m_e = 10^{-3}$. The effective temperature rescaling again dominates the total change. Around $z \simeq 1000$, the total effect is $\simeq 2.5$ times smaller than for $\Delta\alpha/\alpha = 10^{-3}$ mainly due to the weaker dependence of the level energy on m_e . The figure was taken from [34].

1.2.2 Ionization history modifications due to variation of m_e

We now briefly illustrate the changes caused by the effective electron mass, with the variation parametrized as $m_e = m_{e,0}(1 + \Delta m_e/m_e)$ with respect to the standard value $m_{e,0}$. Inspecting the scalings of Eq. (1.1), one expects the overall effect to be smaller than for α_{EM} , but otherwise very comparable. For example, the effect of temperature rescaling should be roughly half as large. Similarly, the effect due to rescaling $A_{2\gamma}$ should be roughly 8 times smaller, and so on. This is in good agreement with our findings (cf. Fig. 1.3).

The net effect on X_e is about 2.5 times smaller than for α_{EM} around $z \simeq 1000$. This suggests that the CMB constraint on m_e is weakened by a similar factor. However, adding the rescaling of the Thomson cross section for the computation of the visibility function strongly enhances the geometric degeneracy for m_e , such that the CMB only constraint on m_e is $\gtrsim 20$ times weaker than for α_{EM} (see Sect. 1.3). In addition, a small difference related to the renormalizations of the photoionization and recombination rates (blue/dashed line) appears. For $\Delta m_e/m_e > 0$, the photoionization rate is increased and the recombination rate is reduced for these contributions [cf. Eq. (1.1)]. Both effects delay recombination (see Fig. 1.3). Thus, around $z \simeq 10^3$ the net effect is slightly larger than for α_{EM} . In contrast to α_{EM} , at late times no net acceleration of recombination occurs. These effects slightly modify the overall red-

shift dependence of the total X_e change, in addition to lowering the effect in the freeze-out tail. At the level $\Delta m_e/m_e \simeq 1\%$, additional higher order terms become important, allowing one to break the near degeneracy between α_{EM} and m_e in joint analyses [68]. At the level of the current CMB only constraints, this aspect indeed is of relevance (Sect. 1.3.2).

1.2.3 Comparison with `CosmoRec` and generalized VFC models.

We highlight that [34] also explicitly demonstrated that a full treatment of the problem using the advanced recombination code `CosmoRec` yields results that are very similar to those from a simpler three-level treatment with correction function approach [88] to mimic the recombination physics corrections. This also allowed [34] to perform calculations with explicit time-dependence of α_{EM} and m_e , initially focusing on a simple power-law redshift dependence

$$\alpha_{\text{EM}}(z) = \alpha_{\text{EM}}(z_0) \left(\frac{1+z}{1100} \right)^p, \quad (1.2)$$

for α_{EM} and similarly for m_e . Using a principal component analysis (PCA) [37], which extended the previous recombination perturbation framework developed in [29, 30, 35], general VFC variations around the recombination era were further studied. This showed that time-dependence can in fact be independently constrained already with existing data and also led to various generalized limits on VFCs during recombination [55, 93], which we will briefly highlight below.

1.3 CMB anisotropy constraints

1.3.1 Propagating the effects to the CMB anisotropies

The temperature and polarization power spectra of the CMB depend on the dynamics of recombination through the ionization history, which defines the Thomson visibility function and last scattering surface [92, 66, 44]. Therefore, variations of α_{EM} and m_e can leave a direct imprint on the CMB power spectra. A detailed description of changes to the visibility function and various additional illustrations also for time-dependent VFCs can be found in [34, 37]. Here, we highlight the changes to the CMB temperature power spectra for variations of α_{EM} and m_e , noting that those in polarization show very similar features. The power spectra were computed using `CAMB` [57] for the standard cosmology [67].

To propagate the effect of VFCs to the CMB anisotropies, two changes are required. The standard recombination history has to be replaced as explained in the previous section. In addition, the Thomson scattering rate has to be updated in the

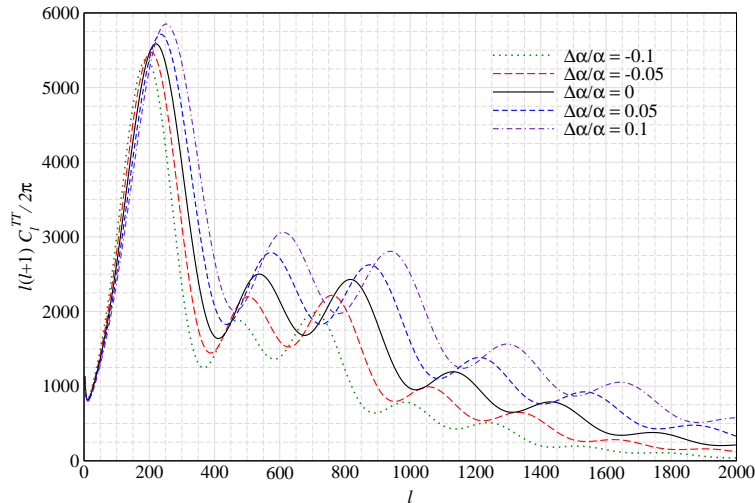


Fig. 1.4: The CMB temperature power spectra for different values of α_{EM} . This shows that as the fine structure constant increases, the anisotropies shift toward smaller scales and higher amplitudes. The figure was taken from [34].

Boltzmann code using the modified Thomson cross section. For the latter, two approaches are possible, one based on directly modifying the Boltzmann code, the other on mimicking the effect by rescaling the ionization history. Both seem to deliver consistent final results [34]. However, we stress how important it is to include the changes to the Thomson scattering rate, as without this effect α_{EM} and m_e variations essentially exhibit a very similar phenomenology [34, 36].

In Fig. 1.4, we illustrate the effect of α_{EM} on the CMB temperature power spectrum. Two main features are visible: Firstly, the peaks of the power spectrum are shifted to smaller scales (larger ℓ) when $\Delta\alpha/\alpha > 0$. This happens because earlier recombination moves the last scattering surface towards higher redshifts, which decreases the sound horizon and increases the angular diameter distance to recombination [48, 8]. Secondly, for $\Delta\alpha/\alpha > 0$, the peak amplitudes are enhanced. This is mainly because earlier recombination suppresses the effect of photon diffusion damping on the anisotropies [48, 8]. For variations of m_e , very similar responses are found, but with an amplitude that is reduced by a factor of $\simeq 2 - 3$ [34].

For small $\Delta\alpha/\alpha$ and $\Delta m_e/m_e$, we illustrate the relative change of the temperature power spectrum in Fig. 1.5. The effect on the peak positions is more noticeable than the small overall tilt caused by changes related to diffusion damping. As expected, the changes to the CMB TT power spectra, $\Delta C_\ell/C_\ell(\Delta\alpha/\alpha)$ and $\Delta C_\ell/C_\ell(\Delta m_e/m_e)$, become almost indistinguishable when using $\Delta m_e/m_e \approx (2 - 3)\Delta\alpha/\alpha$. This presents a quasi-degeneracy between the two parameters and also suggests that naively the analysis for $\Delta\alpha/\alpha$ could be sufficient to estimate the errors for a corresponding analysis of m_e . However, when constraining m_e , an

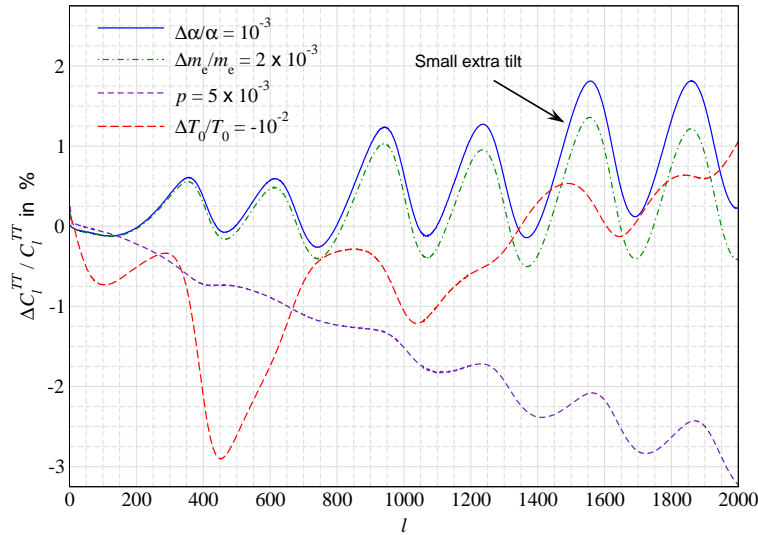


Fig. 1.5: Comparison of the CMB TT power spectrum deviations when varying α_{EM} , m_e , T_0 and p . We chose $\Delta\alpha/\alpha = 10^{-3}$, $\Delta m_e/m_e = 2 \times 10^{-3}$, $\Delta T/T = -10^{-2}$ and $p = 5 \times 10^{-3}$ (simultaneously for α_{EM} and m_e) to obtain effects at a similar level. Notice the small extra tilt when comparing the case for α_{EM} with m_e , which helps when constraining α_{EM} . The figure was taken from [34].

enhanced geometric degeneracy, because of the differing effect of σ_T , inflates the error to the percent level [68, 34]. In this case, higher order terms become important and the near degeneracy is broken. When also adding information from BAO, the error on m_e is strongly reduced, and a simple scaling of the errors, $\sigma(\Delta m_e/m_e) \simeq 3\sigma(\Delta\alpha/\alpha)$, is recovered [34].

In Fig. 1.5, we also illustrate the effect of varying the average CMB temperature, T_0 , and a time-dependent model for both α_{EM} and m_e with a phenomenological power-law as in Eq. (1.2) around a pivot redshift of $z = 1100$. Changes in the CMB monopole temperature show a different response pattern than VFCs, making these two effects principally distinguishable. This is because varying the CMB temperature affects the ionization history (at leading order like VFCs), but without changing the Thomson scattering rate. In addition, T_0 modifies the matter-radiation equality and therefore has a separate overall effect. Similarly, we conclude that the power-law index of the time-dependent model can be independently constrained [34].

Parameter	<i>Planck</i> 2018	<i>Planck</i> 2018	<i>Planck</i> 2018
		+ varying α_{EM}	+ varying m_e
$\Omega_b h^2$	0.02237 ± 0.00015	0.02236 ± 0.00015	$0.0199^{+0.0012}_{-0.0014}$
$\Omega_c h^2$	0.1199 ± 0.0012	0.1201 ± 0.0014	0.1058 ± 0.0076
$100\theta_{MC}$	1.04088 ± 0.00031	1.0416 ± 0.0034	0.958 ± 0.045
τ	0.0542 ± 0.0074	0.0540 ± 0.0075	0.0512 ± 0.0077
$\ln(10^{10} A_s)$	3.044 ± 0.014	3.043 ± 0.015	3.029 ± 0.017
n_s	0.9649 ± 0.0041	0.9637 ± 0.0070	0.9640 ± 0.0040
$\alpha_{\text{EM}}/\alpha_{\text{EM},0}$	--	1.0005 ± 0.0024	--
$m_e/m_{e,0}$	--	--	0.888 ± 0.059
H_0 [km s ⁻¹ Mpc ⁻¹]	67.36 ± 0.54	67.56 ± 0.99	46^{+9}_{-10}

Table 1.1: Marginalised values of the fine structure constant and effective electron mass α_{EM} and m_e using the *Planck* 2018 data alone. A very wide prior ($H_0 > 20 \text{ km s}^{-1} \text{ Mpc}^{-1}$) for H_0 was used to avoid biasing the marginalised m_e posterior, which affected some of the results of the 2013 analysis [34, 36].

1.3.2 Constraints from Planck

Now that we have developed a detailed understanding about how the CMB anisotropies are affected by changes of α_{EM} and m_e , we can directly consider some of the existing constraints from *Planck*. Early constraints were derived using *Planck* 2013 data in [68]. Aside from additional data (e.g., *Planck* polarization) and improvements in the understanding of systematics and calibration, the later analysis of the *Planck* 2015 data yielded similar constraints [34], although with slightly improved errors.² Here we highlight the latest *Planck* 2018 results, which were obtained in [36]. For details we refer the interested reader to that paper.

In Table 1.1, we summarize some of the *Planck* 2018 constraints on α_{EM} and m_e , including the 2018 baseline *Planck* data, with low- ℓ and high- ℓ data for temperature and *E*-mode polarisation power spectra, along with the lensing data from the same release [70, 71]. The addition of α_{EM} marginally affects the values and errors of the six standard parameters, yielding $\alpha_{\text{EM}}/\alpha_{\text{EM},0} = 1.0005 \pm 0.0024$. In contrast, varying m_e has a strong effect especially on H_0 , shifting it to extremely low values and allowing for a low value of the electron rest mass, $m_e/m_{e,0} = 0.888 \pm 0.059$. This is caused by the small differences in the way m_e affects the CMB power spectra, with a crucial role played by adding changes to σ_T [34, 36]. As we discuss below, this large geometric degeneracy is one of the key ingredients for alleviating the Hubble tension when combined with supernova data.

In Fig. 1.6, we show the two-dimensional posteriors for the constraint on simultaneously varying values of α_{EM} and m_e . For comparison, the contours relating to the 2015 analysis and also combinations with baryon acoustic oscillation (BAO) [3] data are illustrated. The constraints for *Planck* alone exhibit very wide posteriors, with slight differences in the centroids of the 2015 and 2018 constraints. We note

² For a detailed discussion of the effects of various analysis choices we refer to [34].

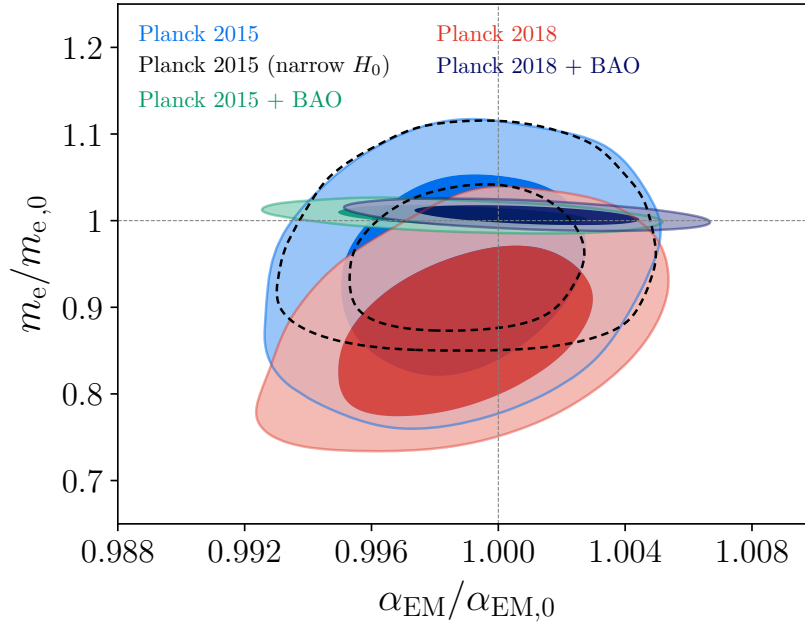


Fig. 1.6: Posterior contours between α_{EM} and m_e for the *Planck* 2015 and 2018 data along with BAO contributions. Note that the dashed contour shows the 2015 contour but with a tighter prior on $H_0 \in \{40, 100\} \text{ km s}^{-1} \text{ Mpc}^{-1}$ to conform with the previous *Planck* 2013 analysis. The figure was taken from [36].

that a narrower prior of $H_0 > 40 \text{ km s}^{-1} \text{ Mpc}^{-1}$ (conforming with the initial CMB analysis of *Planck* [68]) affects the posterior for the 2015 data, shrinking it in the m_e -direction. This further highlights the significant differences in the role of α_{EM} and m_e on the CMB anisotropies.

The introduction of BAO data significantly tightens the constraints on m_e and we can also observe a small drift in the central value of α_{EM} . The obtained value changes from $\alpha_{EM}/\alpha_{EM,0} = 0.9989 \pm 0.0026$ for the 2015 data to $\alpha_{EM}/\alpha_{EM,0} = 1.0010 \pm 0.0024$ with 2018 data, both with BAO included and when simultaneously varying m_e . By contrast, there is no drift for m_e , with $m_e/m_{e,0} = 1.0056 \pm 0.0080$ changing to $m_e/m_{e,0} = 1.0054 \pm 0.0080$ for *Planck* 2015+BAO and *Planck* 2018+BAO, respectively. These findings highlight a strong level of agreement of *Planck* with BAO data, which has been emphasized on many occasions [69].

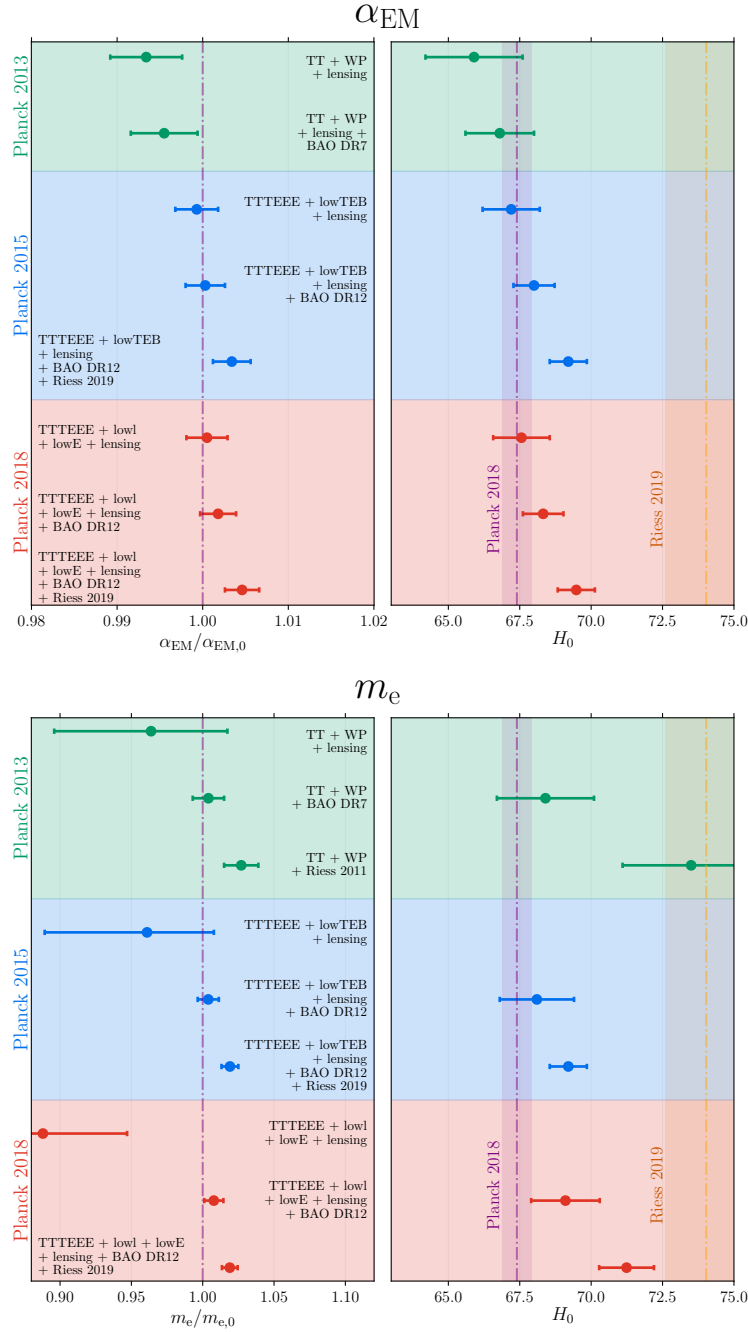


Fig. 1.7: Constraints on the fundamental constants (*left*) using various combinations of *Planck* data together with their H_0 values and errors (*right*). *Top*: results from the fine structure constant α_{EM} . *Bottom*: similar results but from the effective electron mass m_e . Here, we have redacted the constraint for H_0 from CMB data only because the error bars are so large. For the m_e MCMC analysis, we have widened the prior on the Hubble constant such that $H_0 > 20 \text{ km s}^{-1} \text{ Mpc}^{-1}$. Figure is from [36].

1.4 Alleviating the Hubble tension with VFCs

The attentive reader will already have noticed the route forward to alleviating the Hubble tension through varying the electron rest mass. This possibility was first noticed in [36], where the constraints on VFCs from different data combinations were studied, also adding supernova/Cepheid (R19) [74] data.

A summary of the constraints is shown in Fig. 1.7 with particular focus on the interplay with H_0 . For α_{EM} , we can notice broadly consistent constraints across all data combinations with only a small shift in the value of H_0 towards R19 in the combined constraints, indicating a resistance in terms of geometric freedom. For m_e , two effects are found. First, as pointed out above, when adding BAO data, the error on m_e is significantly reduced in comparison to the CMB only constraints, bringing H_0 into agreement with the only CMB inference. Second, when also adding R19, a non-standard value of m_e (at $\simeq 3.5\sigma$ significance) is traded for a reduction of the Hubble tension. This begs the question whether m_e could indeed play a role in this problem. A model comparison study carried out in [82] indeed indicated that a simple variation of m_e provides a good contender in this respect, although not all issues could be resolved.

1.4.1 Adding curvature

As Fig. 1.7 clearly shows, a constant variation of m_e does not fully solve the Hubble tension, albeit reducing it below 2σ . As one possible extension, [36] also studied solutions with power-law VFC time-dependence, but found this to not further improve matters. A little later, [86] studied cosmologies with non-zero curvature in addition to variations of m_e , finding these models to solve the Hubble tension. Indeed, this possibility was the winning finalist in the H_0 -Olympics model comparison exercise [82]. However, allowing for non-zero curvature does open yet another non-standard direction in cosmology (in addition to accepting varying m_e), with strong resistance in terms of standard inflationary predictions [24]. One could feel inclined to cling on to zero curvature cosmologies given the great successes of the inflationary paradigm, but ultimately observations and careful analysis will have to decide.

1.4.2 Time-dependent VFCs models

Most of the results presented above assumed constant (i.e., time-independent/single-valued) changes to the values of FCs in the early Universe. As highlighted in [34], explicitly time-dependent VFCs can in principle be constrained independently even with existing CMB data, given that the CMB responses are distinct (see Fig. 1.5). This idea was later generalized by applying a principal component analysis (PCA) to possible time-dependent VFC perturbations around the standard value in the hopes

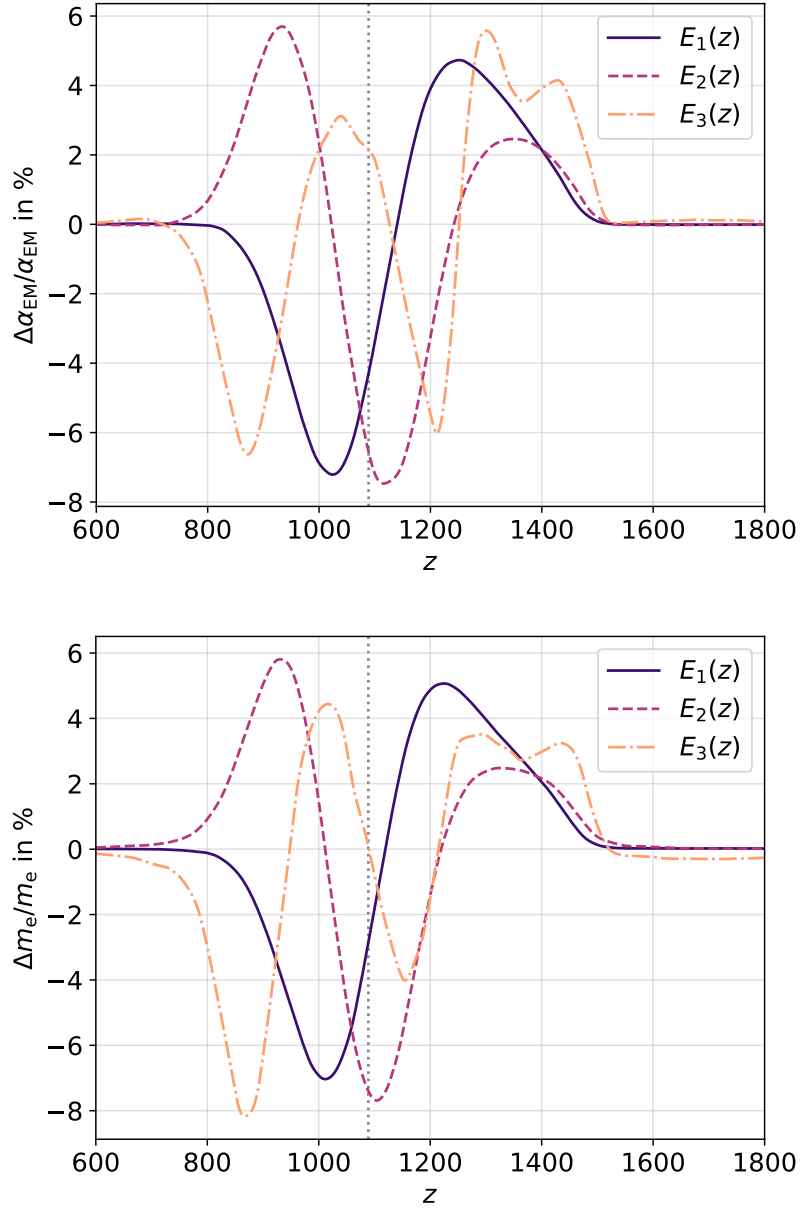


Fig. 1.8: The first three VFC principal components for α_{EM} (top) and m_e (bottom) as constructed using *Planck* 2018 data. The eigenmodes are all normalised such that $\int |E_i^2(z)| dz = 1$. The maximum of the Λ CDM Thomson visibility function has been marked as vertical dotted line. Figure is taken from [37].

to further diminish the Hubble tension [37]. The idea is very simple: given the (CMB) observables, it is difficult to limit a specific change in the values of FCs at a given redshift. However, certain correlated variations/perturbations (i.e., VFC modes) across wider ranges of redshifts can indeed be analyzed and constrained. To construct these VFC eigenmodes, one can use the Fisher information matrix to assess the observability. This yields a ranked system of possible VFC modes that can be best constrained by the data. Similar approaches were applied to studies of perturbations in the reionization [64] and recombination [29, 30, 35] histories.

The first few α_{EM} and m_e eigenmodes are shown in Fig. 1.8. In a perturbative sense, most of the information on VFCs can be gleaned from around the maximum of the Thomson visibility at $z \simeq 1100$. This is reflected in the localization of the VFC modes around this redshift. Applying these VFC modes to the *Planck* 2018 data no significant detection of non-zero mode amplitudes was found [37]. Similarly, when combining with BAO and R19, no additional improvement with respect to the Hubble tension over a constant variation was identified [37]. However, to exclude the possibility of a more general time-dependent VFC history, this would require further investigations of time-dependent models that interface between the standard candle, low-redshift era and the surface of last scattering.

The PCA approach inherently assumes a perturbative variation of the FCs. This assumption need not hold, and in addition higher order eigenmodes that individually fall below the detection threshold (due to their more rapid redshift-variability) could together allow for more general modifications [30]. In [55], an assessment of which time-dependent change to α_{EM} and m_e would be required to reduce the Hubble tension was carried out. It was demonstrated that more general time-dependent variations of α_{EM} and m_e around recombination can solve the Hubble tension (and even reduce the S_8 tension) when applied to CMB data alone. However, once BAO and supernova data is added, full solutions to the Hubble tension evade a perturbative treatment, although extension of the framework to the non-perturbative regime can be done [55]. This points towards the possibility that more general theoretical models could indeed help to restore consistency between various probes, although more work is certainly needed.

1.5 New insights from the cosmological recombination radiation

In the previous sections, we have primarily focused on illustrating the role of VFCs, and in particular of m_e , in possible solutions to the Hubble tension. In this, one key ingredient is the associated modification to the cosmological recombination history, although it seems clear that a simple perturbative change does not provide a sufficient degree of freedom to fully resolve the tension. However, stepping back from a VFC driven solution, one important question is how we could tell if indeed a (strongly) modified recombination history is responsible for the Hubble tension? Furthermore, solutions based on PMFs (see [47]) are also mainly successful because

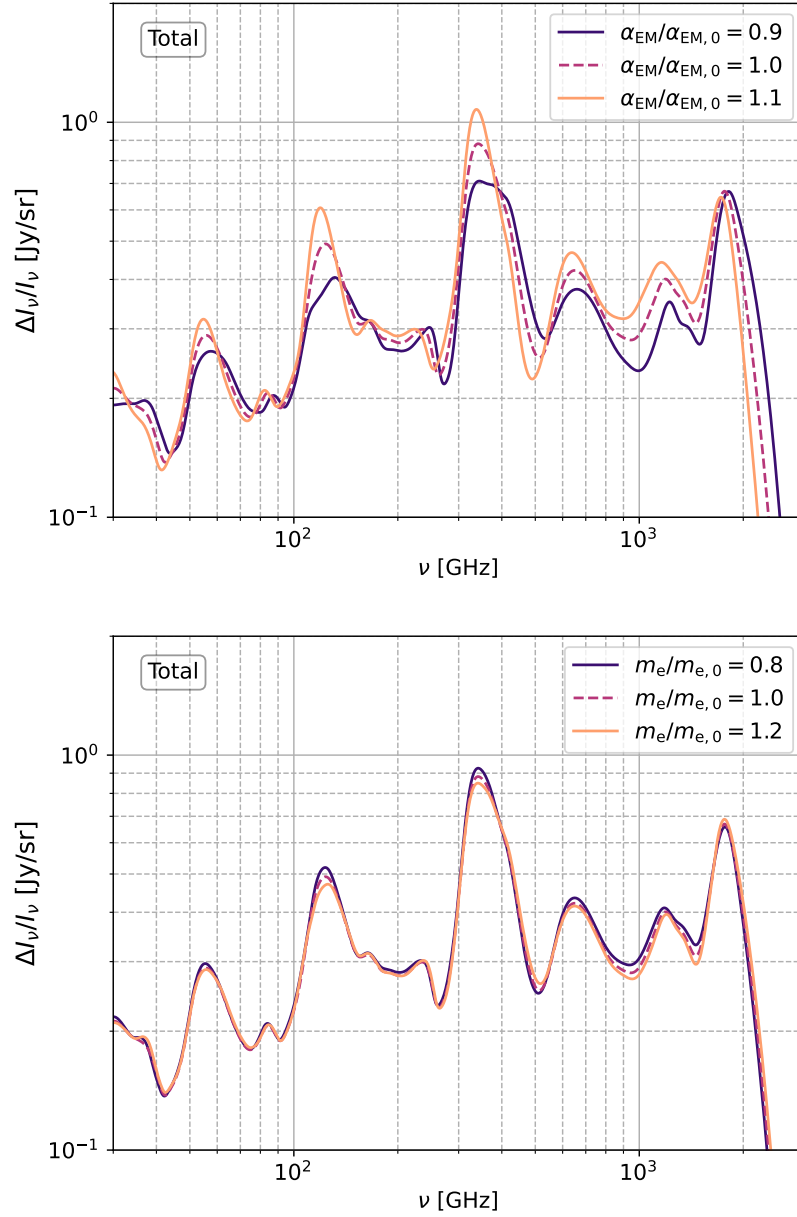


Fig. 1.9: The total impact on the recombination lines from the variations for $\Delta\alpha_{EM}/\alpha_{EM,0} = \pm 0.1$ (top). The total variations due to changes in $\Delta m_e/m_{e,0} = \pm 0.2$ are shown for comparison (bottom). Figure taken from [38].

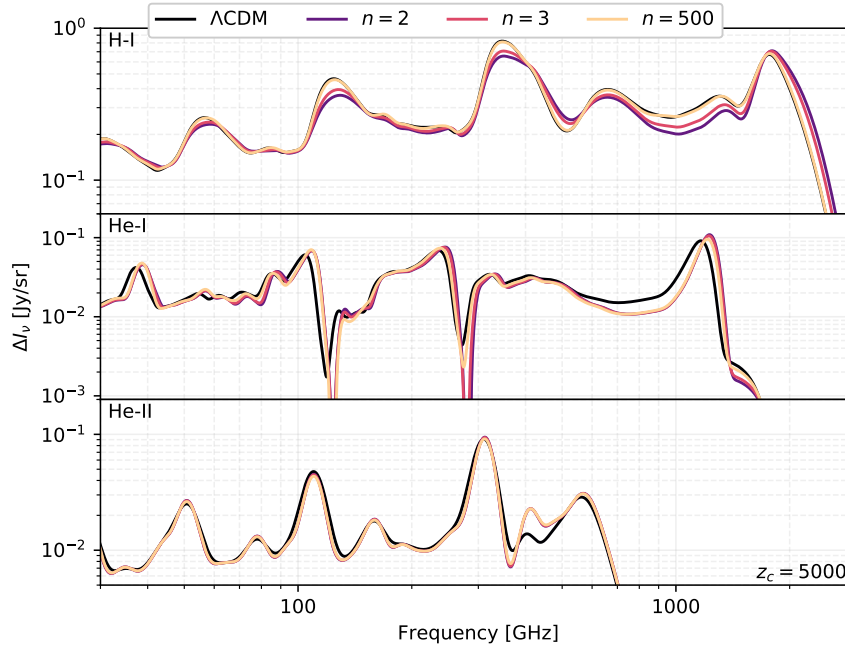


Fig. 1.10: Comparison for an EDE model that has different slopes for $z_c = 5000$ across the different atomic species. Hydrogen (*top*) is compared against the Helium I and II (*middle, bottom*) lines, respectively. For better clarity, this has been plotted with $f_{\text{ede}} = 0.8$. Figure taken from [38].

of their modifications to the average recombination history. It is thus important to ask how could we distinguish different options?

One important avenue forward is to use more accurate measurements with upcoming CMB experiments such as The Simons Observatory [2] and CMB-S4 [1] to improve the constraints on VFC [36, 37]. However, ultimately access to new observables will be required.

The cosmological recombination processes is also associated with the emission of photons from the Hydrogen and Helium plasma [27, 80, 28, 13, 50, 79, 17, 78]. The cosmological recombination radiation (CRR) can now be accurately computed using `CosmoSpec` [15], which was extended to also incorporate the effect of VFCs [38]. This CMB distortion signal may become observable [39] with future CMB spectrometers akin to *PIXIE* [53, 52, 14], opening the exciting possibility to directly study the dynamics of the recombination process [20, 91].

In Fig. 1.9, we illustrate the effect of varying α_{EM} and m_e on the CRR. Firstly, one can clearly see that for the chosen parameters there is a noticeable effect on the amplitude and position of the CRR features. For α_{EM} , the modifications are more pronounced, which in part is due to a near degeneracy of m_e with modifications

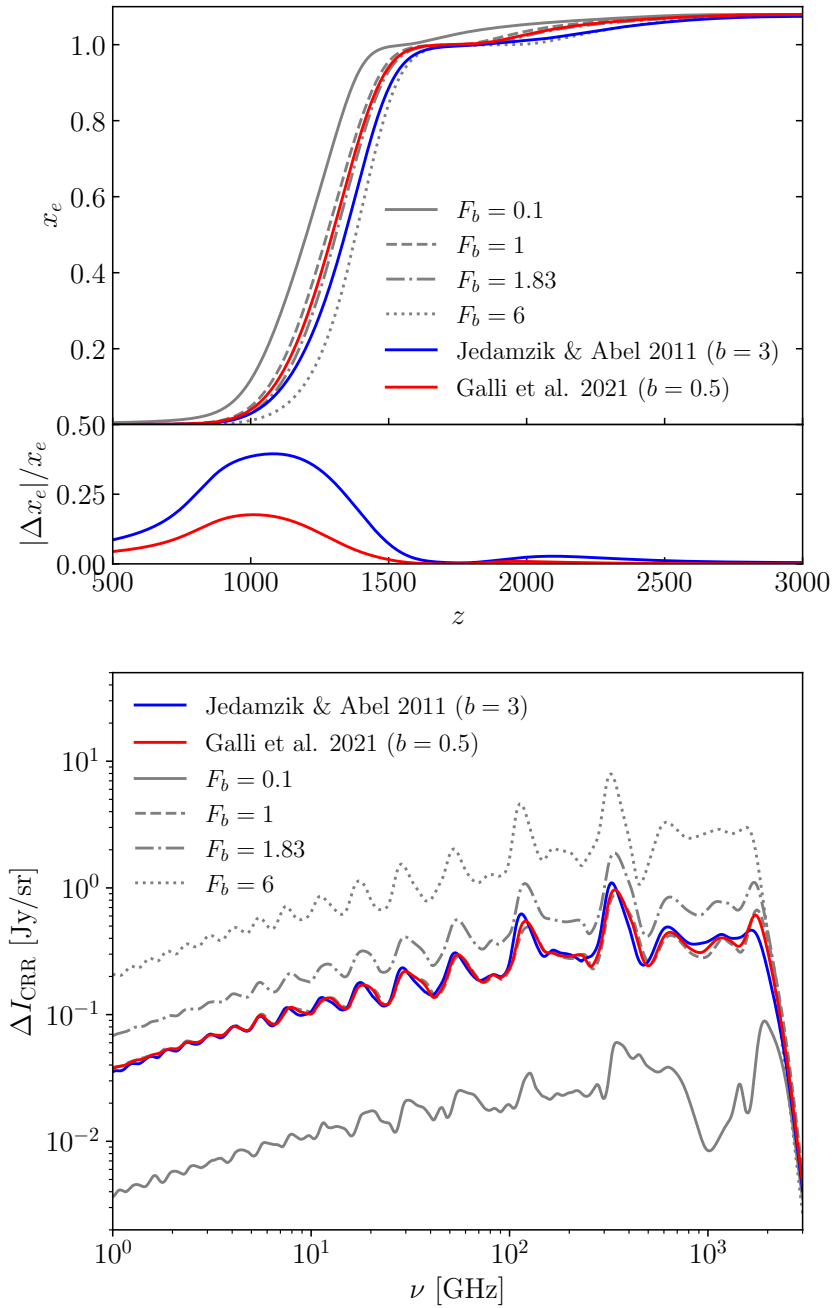


Fig. 1.11: Recombination histories (upper panel) and CRR spectra (lower panel) for the PMF models similar to those consider in [45, 46, 32]. The individual spectra for various values of the baryon density enhancement factor are shown as gray lines (the $F_b = 1$ case corresponds to Λ CDM). The averages are instead displayed in blue and red, and show significant second order contributions, manifesting in smearing of the lines and shifts in their position.

to the time of recombination [38]. Nevertheless, it is clear that precision measurements of the average CMB spectrum could principally identify these modifications in comparison to the standard Λ CDM prediction, thereby shedding new light on the physical cause of the problem.

However, we would like to highlight that these novel opportunities are not limited to searches for VFCs. Also EDE models (see [72, 73]) indirectly affect the shape of the CRR [38]. In Fig. 1.10, we illustrate the effect of EDE on the CRR. Importantly, depending on the parameter choices [38], the redshifting between the Hydrogen and Helium recombination lines can be modified in addition to when the lines are created. This leads to principally observable features in the CRR, would a sufficient spectral sensitivity be reached. Finally, small-scale perturbations in the baryonic density, as possibly induced by PMFs (see [47]), can leave an imprint to the CRR that could be used to identify this process (see Fig. 1.11). Physically, the modifications are simply related to the fact that the average CRR is no longer given by the CRR of the average parameters, as non-linear (non-perturbative) corrections to the recombination process remain. Overall, all these examples illustrate that future CMB spectral distortion measurements could in principle allow us to directly test the underlying recombination process. From the scientific point of view it would actually be crucial to investigate the recombination history directly, thereby eliminating one of the remaining theoretical ingredients of in CMB cosmology. However, it is also clear that due to the presence of foregrounds the required spectral sensitivity and coverage are still quite futuristic [81, 23, 39]. In addition, a control of systematics and removal of foregrounds will have to be performed to unprecedented precision. These challenges will remain to be solved by generations of cosmologists to come.

1.6 Conclusions

In this chapter, we illustrated the role of VFCs in the Hubble tension. Previous studies have shown that varying m_e could indeed offer viable solutions, although no VFC scenario could fully resolve all aspects of the tension. It is however important to note that additional studies in the non-perturbative regime (i.e., significant changes with explicit time-dependence) could further improve the consistency. In addition, so far no attempt has been made to simultaneously treat VFCs and EDE, although both could principally originate from the same scalar field. With the advent of improved cosmological data, these lines of research might become very interesting.

One obvious question remains: how can we ultimately distinguish between various solutions to the Hubble tension. As highlighted in Sect. 1.5, EDE, PMFs and VFCs can in principle also be (directly) constrained through detailed measurements of the CRR. This guaranteed Λ CDM signal may become observable in the future with advanced CMB spectrometers and would open a way to confront our understanding of the cosmological recombination process with direct observational evidence. Should the Hubble tension not be resolved in the next decades, this future probe might be one of the important avenues towards a final primordial test.

Acknowledgements We thank Yacine Ali-Haïmoud for useful comments on the manuscript. This work was supported by the ERC Consolidator Grant *CMBSPEC* (No. 725456). JC was furthermore supported by the Royal Society as a Royal Society University Research Fellow at the University of Manchester, UK (No. URF/R/191023). Part of this work was carried out in the stimulating and peaceful environment offered at the Aspen Center for Physics, which is supported by the National Science Foundation grant PHY-2210452.

References

1. K. N. Abazajian, P. Adshead, Z. Ahmed, S. W. Allen, D. Alonso, K. S. Arnold, C. Baccigalupi, J. G. Bartlett, N. Battaglia, B. A. Benson, C. A. Bischoff, J. Borrill, V. Buza, E. Calabrese, R. Caldwell, J. E. Carlstrom, C. L. Chang, T. M. Crawford, F.-Y. Cyr-Racine, F. De Bernardis, T. de Haan, S. di Serego Alighieri, J. Dunkley, C. Dvorkin, J. Errard, G. Fabbian, S. Feeney, S. Ferraro, J. P. Filippini, R. Flauger, G. M. Fuller, V. Gluscevic, D. Green, D. Grin, E. Grohs, J. W. Henning, J. C. Hill, R. Hlozek, G. Holder, W. Holzappel, W. Hu, K. M. Huffenberger, R. Keskitalo, L. Knox, A. Kosowsky, J. Kovac, E. D. Kovetz, C.-L. Kuo, A. Kusaka, M. Le Jeune, A. T. Lee, M. Lilley, M. Loverde, M. S. Madhavacheril, A. Mantz, D. J. E. Marsh, J. McMahon, P. D. Meerburg, J. Meyers, A. D. Miller, J. B. Munoz, H. N. Nguyen, M. D. Niemack, M. Peloso, J. Peloton, L. Pogosian, C. Pryke, M. Raveri, C. L. Reichardt, G. Rocha, A. Rotti, E. Schaan, M. M. Schmittfull, D. Scott, N. Sehgal, S. Shandera, B. D. Sherwin, T. L. Smith, L. Sorbo, G. D. Starkman, K. T. Story, A. van Engelen, J. D. Vieira, S. Watson, N. Whitehorn, and W. L. Kimmy Wu. CMB-S4 Science Book, First Edition. *ArXiv:1610.0274*, Oct. 2016.
2. P. Ade, J. Aguirre, Z. Ahmed, S. Aiola, A. Ali, D. Alonso, M. A. Alvarez, K. Arnold, P. Ashton, J. Austermann, H. Awan, C. Baccigalupi, T. Baidon, D. Barron, N. Battaglia, R. Battye, E. Baxter, A. Bazarko, J. A. Beall, R. Bean, D. Beck, S. Beckman, B. Beringue, F. Bianchini, S. Boada, D. Boettger, J. R. Bond, J. Borrill, M. L. Brown, S. M. Bruno, S. Bryan, E. Calabrese, V. Calafut, P. Calisse, J. Carron, A. Challinor, G. Chesmore, Y. Chinone, J. Chluba, H.-M. S. Cho, S. Choi, G. Coppi, N. F. Cothard, K. Coughlin, D. Crichton, K. D. Crowley, K. T. Crowley, A. Cukierman, J. M. D’Ewart, R. Dünner, T. de Haan, M. Devlin, S. Dicker, J. Didier, M. Dobbs, B. Dober, C. J. Duell, S. Duff, A. Duivenvoorden, J. Dunkley, J. Dusatko, J. Errard, G. Fabbian, S. Feeney, S. Ferraro, P. Fluxà, K. Freese, J. C. Frisch, A. Frolov, G. Fuller, B. Fuzia, N. Galitzki, P. A. Gallardo, J. Tomás Galvez Gherzi, J. Gao, E. Gawiser, M. Gerbino, V. Gluscevic, N. Goeckner-Wald, J. Golec, S. Gordon, M. Gralla, D. Green, A. Grigorian, J. Groh, C. Groppi, Y. Guan, J. E. Gudmundsson, D. Han, P. Hargrave, M. Hasegawa, M. Hasselfield, M. Hattori, V. Haynes, M. Hazumi, Y. He, E. Healy, S. W. Henderson, C. Hervias-Caimapo, C. A. Hill, J. C. Hill, G. Hilton, M. Hilton, A. D. Hincks, G. Hinshaw, R. Hložek, S. Ho, S.-P. P. Ho, L. Howe, Z. Huang, J. Hubmayr, K. Huffenberger, J. P. Hughes, A. Ijjas, M. Ikape, K. Irwin, A. H. Jaffe, B. Jain, O. Jeong, D. Kaneko, E. D. Karpel, N. Katayama, B. Keating, S. S. Kernasovskiy, R. Keskitalo, T. Kisner, K. Kiuchi, J. Klein, K. Knowles, B. Koopman, A. Kosowsky, N. Krachmalnicoff, S. E. Kuenstner, C.-L. Kuo, A. Kusaka, J. Lashner, A. Lee, E. Lee, D. Leon, J. S. Y. Leung, A. Lewis, Y. Li, Z. Li, M. Limon, E. Linder, C. Lopez-Caraballo, T. Louis, L. Lowry, M. Lungu, M. Madhavacheril, D. Mak, F. Maldonado, H. Mani, B. Mates, F. Matsuda, L. Maurin, P. Mäuskopf, A. May, N. McCallum, C. McKenney, J. McMahon, P. D. Meerburg, J. Meyers, A. Miller, M. Mirmelstein, K. Moodley, M. Munchmeyer, C. Munson, S. Naess, F. Nati, M. Navaroli, L. Newburgh, H. N. Nguyen, M. Niemack, H. Nishino, J. Orłowski-Scherer, L. Page, B. Partridge, J. Peloton, F. Perrotta, L. Piccirillo, G. Pisano, D. Poletti, R. Puddu, G. Puglisi, C. Raun, C. L. Reichardt, M. Remazeilles, Y. Rephaeli, D. Riechers, F. Rojas, A. Roy, S. Sadeh, Y. Sakurai, M. Salatino, M. Sathyanarayana Rao, E. Schaan, M. Schmittfull, N. Sehgal, J. Seibert, U. Seljak, B. Sherwin, M. Shimon, C. Sierra, J. Sievers, P. Sikhosana, M. Silva-Feaver, S. M. Simon,

- A. Sinclair, P. Siritanasak, K. Smith, S. R. Smith, D. Spergel, S. T. Staggs, G. Stein, J. R. Stevens, R. Stompor, A. Suzuki, O. Tajima, S. Takakura, G. Teply, D. B. Thomas, B. Thorne, R. Thornton, H. Trac, C. Tsai, C. Tucker, J. Ullom, S. Vagnozzi, A. van Engelen, J. Van Lanen, D. D. Van Winkle, E. M. Vavagiakis, C. Vergès, M. Vissers, K. Wagoner, S. Walker, J. Ward, B. Westbrook, N. Whitehorn, J. Williams, J. Williams, E. J. Wollack, Z. Xu, B. Yu, C. Yu, F. Zago, H. Zhang, N. Zhu, and Simons Observatory Collaboration. The Simons Observatory: science goals and forecasts. *JCAP*, 2019(2):056, Feb. 2019.
3. S. Alam, F. D. Albareti, C. A. Prieto, F. Anders, S. F. Anderson, T. Anderton, B. H. Andrews, E. Armengaud, A. Aubourg, S. Bailey, and et al. The eleventh and twelfth data releases of the sloan digital sky survey: Final data from sdss-iii. *The Astrophysical Journal Supplement Series*, 219(1):12, Jul 2015.
 4. Y. Ali-Haïmoud, D. Grin, and C. M. Hirata. Radiative transfer effects in primordial hydrogen recombination. *Phys.Rev.D*, 82(12):123502–+, Dec. 2010.
 5. Y. Ali-Haïmoud and C. M. Hirata. HyRec: A fast and highly accurate primordial hydrogen and helium recombination code. *Phys.Rev.D*, 83(4):043513–+, Feb. 2011.
 6. P. P. Avelino, S. Esposito, G. Mangano, C. J. A. P. Martins, A. Melchiorri, G. Miele, O. Pisanti, G. Rocha, and P. T. P. Viana. Early-universe constraints on a time-varying fine structure constant. *Phys.Rev.D*, 64(10):103505, Nov. 2001.
 7. P. P. Avelino, C. J. A. P. Martins, G. Rocha, and P. Viana. Looking for a varying α in the cosmic microwave background. *Phys.Rev.D*, 62(12):123508, Dec. 2000.
 8. R. A. Battye, R. Crittenden, and J. Weller. Cosmic concordance and the fine structure constant. *Phys.Rev.D*, 63(4):043505, Feb. 2001.
 9. J. D. Bekenstein. Fine-structure constant: Is it really a constant? *Phys. Rev. D*, 25:1527–1539, Mar 1982.
 10. H. A. Bethe and E. E. Salpeter. *Quantum Mechanics of One- and Two-Electron Atoms*. 1957.
 11. S. Bize, S. A. Diddams, U. Tanaka, C. E. Tanner, W. H. Oskay, R. E. Drullinger, T. E. Parker, T. P. Heavner, S. R. Jefferts, L. Hollberg, W. M. Itano, and J. C. Bergquist. Testing the stability of fundamental constants with the $^{199}\text{Hg}^+$ single-ion optical clock. *Phys. Rev. Lett.*, 90:150802, Apr 2003.
 12. P. Bonifacio, H. Rahmani, J. B. Whitmore, M. Wendt, M. Centurion, P. Molaro, R. Srianand, M. T. Murphy, P. Petitjean, I. I. Agafonova, S. D’Odorico, T. M. Evans, S. A. Levshakov, S. Lopez, C. J. A. P. Martins, D. Reimers, and G. Vladilo. Fundamental constants and high-resolution spectroscopy. *Astronomische Nachrichten*, 335:83, Jan. 2014.
 13. M. S. Burgin. Hydrogen Subordinate Line Emission at the Epoch of Cosmological Recombination. *Astronomy Reports*, 47:709–716, Sept. 2003.
 14. J. Chluba, M. H. Abitbol, N. Aghanim, Y. Ali-Haïmoud, M. Alvarez, K. Basu, B. Bolliet, C. Burigana, P. de Bernardis, J. Delabrouille, E. Dimastrogiovanni, F. Finelli, D. Fixsen, L. Hart, C. Hernández-Monteagudo, J. C. Hill, A. Kogut, K. Kohri, J. Lesgourgues, B. Maffei, J. Mather, S. Mukherjee, S. P. Patil, A. Ravenni, M. Remazeilles, A. Rotti, J. A. Rubiño-Martín, J. Silk, R. A. Sunyaev, and E. R. Switzer. New horizons in cosmology with spectral distortions of the cosmic microwave background. *Experimental Astronomy*, 51(3):1515–1554, June 2021.
 15. J. Chluba and Y. Ali-Haïmoud. COSMOSPEC: fast and detailed computation of the cosmological recombination radiation from hydrogen and helium. *MNRAS*, 456:3494–3508, Mar. 2016.
 16. J. Chluba, J. Fung, and E. R. Switzer. Radiative transfer effects during primordial helium recombination. *MNRAS*, 423:3227–3242, July 2012.
 17. J. Chluba and R. A. Sunyaev. Free-bound emission from cosmological hydrogen recombination. *A&A*, 458:L29–L32, Nov. 2006.
 18. J. Chluba and R. A. Sunyaev. Induced two-photon decay of the 2s level and the rate of cosmological hydrogen recombination. *A&A*, 446:39–42, Jan. 2006.
 19. J. Chluba and R. A. Sunyaev. Cosmological hydrogen recombination: Ly α line feedback and continuum escape. *A&A*, 475:109–114, Nov. 2007.
 20. J. Chluba and R. A. Sunyaev. Is there a need and another way to measure the cosmic microwave background temperature more accurately? *A&A*, 478:L27–L30, Feb. 2008.

21. J. Chluba and R. A. Sunyaev. Time-dependent corrections to the Ly α escape probability during cosmological recombination. *A&A*, 496:619–635, Mar. 2009.
22. J. Chluba and R. M. Thomas. Towards a complete treatment of the cosmological recombination problem. *MNRAS*, 412:748–764, Apr. 2011.
23. V. Desjacques, J. Chluba, J. Silk, F. de Bernardis, and O. Doré. Detecting the cosmological recombination signal from space. *MNRAS*, 451:4460–4470, Aug. 2015.
24. E. Di Dio, F. Montanari, A. Raccanelli, R. Durrer, M. Kamionkowski, and J. Lesgourgues. Curvature constraints from large scale structure. *JCAP*, 2016(6):013, June 2016.
25. G. W. F. Drake. *Springer Handbook of Atomic, Molecular, and Optical Physics*. Springer, 2006.
26. G. W. F. Drake and D. C. Morton. A Multiplet Table for Neutral Helium ($^4\text{He I}$) with Transition Rates. *ApJS*, 170:251–260, May 2007.
27. V. K. Dubrovich. Hydrogen recombination lines of cosmological origin. *Soviet Astronomy Letters*, 1:196–+, Oct. 1975.
28. V. K. Dubrovich and V. A. Stolyarov. Fossil radio lines of hydrogen in the cosmic background radiation at decimeter and meter wavelengths. *A&A*, 302:635–+, Oct. 1995.
29. M. Farhang, J. R. Bond, and J. Chluba. Semi Blind Eigen Analyses of Recombination Histories Using Cosmic Microwave Background Data. *ApJ*, 752:88, June 2012.
30. M. Farhang, J. R. Bond, J. Chluba, and E. R. Switzer. Constraints on Perturbations to the Recombination History from Measurements of the Cosmic Microwave Background Damping Tail. *ApJ*, 764:137, Feb. 2013.
31. W. A. Fendt, J. Chluba, J. A. Rubiño-Martín, and B. D. Wandelt. RICO: A New Approach for Fast and Accurate Representation of the Cosmological Recombination History. *ApJS*, 181:627–638, Apr. 2009.
32. S. Galli, L. Pogosian, K. Jedamzik, and L. Balkenhol. Consistency of Planck, ACT, and SPT constraints on magnetically assisted recombination and forecasts for future experiments. *Phys. Rev. D*, 105(2):023513, 2022.
33. S. C. O. Glover, J. Chluba, S. R. Furlanetto, J. R. Pritchard, and D. W. Savin. Chapter Three - Atomic, Molecular, and Optical Physics in the Early Universe: From Recombination to Reionization. *Advances in Atomic Molecular and Optical Physics*, 63:135–270, Aug. 2014.
34. L. Hart and J. Chluba. New constraints on time-dependent variations of fundamental constants using planck data. *MNRAS*, 474(2):1850–1861, 2018.
35. L. Hart and J. Chluba. Improved model-independent constraints on the recombination era and development of a direct projection method. *MNRAS*, 495(4):4210–4226, July 2020.
36. L. Hart and J. Chluba. Updated fundamental constant constraints from Planck 2018 data and possible relations to the Hubble tension. *MNRAS*, 493(3):3255–3263, Apr. 2020.
37. L. Hart and J. Chluba. Varying fundamental constants principal component analysis: additional hints about the Hubble tension. *MNRAS*, 510(2):2206–2227, Feb. 2022.
38. L. Hart and J. Chluba. Using the cosmological recombination radiation to probe early dark energy and fundamental constant variations. *MNRAS*, 519(3):3664–3680, Mar. 2023.
39. L. Hart, A. Rotti, and J. Chluba. Sensitivity forecasts for the cosmological recombination radiation in the presence of foregrounds. *MNRAS*, 497(4):4535–4548, Oct. 2020.
40. C. M. Hirata. Two-photon transitions in primordial hydrogen recombination. *Phys.Rev.D*, 78(2):023001–+, July 2008.
41. K. Hoshiya and Y. Toda. Electron mass variation from dark sector interactions and compatibility with cosmological observations. *Phys.Rev.D*, 107(4):043505, Feb. 2023.
42. W. Hu, D. Scott, N. Sugiyama, and M. White. Effect of physical assumptions on the calculation of microwave background anisotropies. *Phys.Rev.D*, 52:5498–5515, Nov. 1995.
43. W. Hu and N. Sugiyama. Anisotropies in the cosmic microwave background: an analytic approach. *ApJ*, 444:489–506, May 1995.
44. W. Hu and N. Sugiyama. Small-Scale Cosmological Perturbations: an Analytic Approach. *ApJ*, 471:542, Nov. 1996.
45. K. Jedamzik and T. Abel. Small-scale primordial magnetic fields and anisotropies in the cosmic microwave background radiation. *JCAP*, 10:050, 2013.

46. K. Jedamzik and L. Pogosian. Relieving the Hubble tension with primordial magnetic fields. *Phys. Rev. Lett.*, 125(18):181302, 2020.
47. K. Jedamzik and L. Pogosian. Primordial magnetic fields and the Hubble tension. *arXiv e-prints*, page arXiv:2307.05475, July 2023.
48. M. Kaplinghat, R. J. Scherrer, and M. S. Turner. Constraining variations in the fine-structure constant with the cosmic microwave background. *Phys.Rev.D*, 60(2):023516–+, July 1999.
49. W. J. Karzas and R. Latter. Electron Radiative Transitions in a Coulomb Field. *ApJS*, 6:167–+, May 1961.
50. E. E. Kholupenko, A. V. Ivanchik, and D. A. Varshalovich. *Gravitation and Cosmology*, 11:161–165, 2005.
51. E. E. Kholupenko, A. V. Ivanchik, and D. A. Varshalovich. Rapid HeII-HeI recombination and radiation arising from this process. *MNRAS*, 378:L39–L43, June 2007.
52. A. Kogut and D. J. Fixsen. Foreground Bias from Parametric Models of Far-IR Dust Emission. *ApJ*, 826:101, Aug. 2016.
53. A. Kogut, D. J. Fixsen, D. T. Chuss, J. Dotson, E. Dwek, M. Halpern, G. F. Hinshaw, S. M. Meyer, S. H. Moseley, M. D. Seiffert, D. N. Spergel, and E. J. Wollack. The Primordial Inflation Explorer (PIXIE): a nulling polarimeter for cosmic microwave background observations. *JCAP*, 7:25–+, July 2011.
54. S. M. Kotuš, M. T. Murphy, and R. F. Carswell. High-precision limit on variation in the fine-structure constant from a single quasar absorption system. *Monthly Notices of the Royal Astronomical Society*, 464(3):3679, 2017.
55. N. Lee, Y. Ali-Haïmoud, N. Schöneberg, and V. Poulin. What It Takes to Solve the Hubble Tension through Modifications of Cosmological Recombination. *Phys.Rev.Lett*, 130(16):161003, Apr. 2023.
56. J. Lesgourgues. The Cosmic Linear Anisotropy Solving System (CLASS) I: Overview. *ArXiv:1104.2932*, Apr. 2011.
57. A. Lewis, A. Challinor, and A. Lasenby. Efficient Computation of Cosmic Microwave Background Anisotropies in Closed Friedmann-Robertson-Walker Models. *ApJ*, 538:473–476, Aug. 2000.
58. A. Lewis, J. Weller, and R. Battye. The cosmic microwave background and the ionization history of the Universe. *MNRAS*, 373:561–570, Dec. 2006.
59. M. Lucca, J. Chluba, and A. Rotti. CRRfast: An emulator for the Cosmological Recombination Radiation with effects from inhomogeneous recombination. *arXiv e-prints*, page arXiv:2306.08085, June 2023.
60. C. J. A. P. Martins. The status of varying constants: a review of the physics, searches and implications. *Reports on Progress in Physics*, 80(12):126902, Dec. 2017.
61. C. J. A. P. Martins, A. Melchiorri, G. Rocha, R. Trotta, P. P. Avelino, and P. T. P. Viana. WMAP constraints on varying α and the promise of reionization. *Physics Letters B*, 585:29–34, Apr. 2004.
62. C. J. A. P. Martins, P. E. Vielzeuf, M. Martinelli, E. Calabrese, and S. Pandolfi. Evolution of the fine-structure constant in runaway dilaton models. *Phys. Lett.*, B743:377–382, 2015.
63. E. Menegoni, M. Archidiacono, E. Calabrese, S. Galli, C. J. A. P. Martins, and A. Melchiorri. Fine structure constant and the CMB damping scale. *Phys.Rev.D*, 85(10):107301, May 2012.
64. M. J. Mortonson, C. Dvorkin, H. V. Peiris, and W. Hu. CMB polarization features from inflation versus reionization. *Phys.Rev.*, D79:103519, 2009.
65. P. J. E. Peebles. Recombination of the Primeval Plasma. *ApJ*, 153:1–+, July 1968.
66. P. J. E. Peebles and J. T. Yu. Primeval Adiabatic Perturbation in an Expanding Universe. *ApJ*, 162:815–+, Dec. 1970.
67. Planck Collaboration, P. A. R. Ade, N. Aghanim, M. Arnaud, M. Ashdown, J. Aumont, C. Baccigalupi, A. J. Banday, R. B. Barreiro, J. G. Bartlett, and et al. Planck 2015 results. XIII. Cosmological parameters. *ArXiv:1502.01589*, Feb. 2015.
68. Planck Collaboration, P. A. R. Ade, N. Aghanim, M. Arnaud, M. Ashdown, J. Aumont, C. Baccigalupi, A. J. Banday, R. B. Barreiro, E. Battaner, K. Benabed, A. Benoit-Lévy, J.-P. Bernard, M. Bersanelli, P. Bielewicz, J. R. Bond, J. Borrill, F. R. Bouchet, C. Burigana,

- R. C. Butler, E. Calabrese, A. Chamballu, H. C. Chiang, P. R. Christensen, D. L. Clements, L. P. L. Colombo, F. Couchot, A. Curto, F. Cuttaia, L. Danese, R. D. Davies, R. J. Davis, P. de Bernardis, A. de Rosa, G. de Zotti, J. Delabrouille, J. M. Diego, H. Dole, O. Doré, X. Dupac, T. A. Enßlin, H. K. Eriksen, O. Fabre, F. Finelli, O. Forni, M. Frailis, E. Franceschi, S. Galeotta, S. Galli, K. Ganga, M. Giard, J. González-Nuevo, K. M. Górski, A. Gregorio, A. Gruppuso, F. K. Hansen, D. Hanson, D. L. Harrison, S. Henrot-Versillé, C. Hernández-Monteagudo, D. Herranz, S. R. Hildebrandt, E. Hivon, M. Hobson, W. A. Holmes, A. Hornstrup, W. Hovest, K. M. Huffenberger, A. H. Jaffe, W. C. Jones, E. Keihänen, R. Keskitalo, R. Kneissl, J. Knoche, M. Kunz, H. Kurki-Suonio, J.-M. Lamarre, A. Lasenby, C. R. Lawrence, R. Leonardi, J. Lesgourgues, M. Liguori, P. B. Lilje, M. Linden-Vørnle, M. López-Caniago, P. M. Lubin, J. F. Macías-Pérez, N. Mandolesi, M. Maris, P. G. Martin, E. Martínez-González, S. Masi, S. Matarrese, P. Mazzotta, P. R. Meinhold, A. Melchiorri, L. Mendes, E. Menegoni, A. Mennella, M. Migliaccio, M.-A. Miville-Deschênes, A. Moneti, L. Montier, G. Morgante, A. Moss, D. Munshi, J. A. Murphy, P. Naselsky, F. Nati, P. Natoli, H. U. Nørgaard-Nielsen, F. Noviello, D. Novikov, I. Novikov, C. A. Oxborrow, L. Pagano, F. Pajot, D. Paoletti, F. Pasian, G. Patanchon, O. Perdereau, L. Perotto, F. Perrotta, F. Piacentini, M. Piat, E. Pierpaoli, D. Pietrobon, S. Plaszczyński, E. Pointecouteau, G. Polenta, N. Ponthieu, L. Popa, G. W. Pratt, S. Prunet, J. P. Rachen, R. Rebolo, M. Reinecke, M. Remazeilles, C. Renault, S. Ricciardi, I. Ristorcelli, G. Rocha, G. Roudier, B. Rusholme, M. Sandri, G. Savini, D. Scott, L. D. Spencer, V. Stolyarov, R. Sudiwala, D. Sutton, A.-S. Suur-Uski, J.-F. Sygnet, J. A. Tauber, D. Tavagnacco, L. Terenzi, L. Toffolatti, M. Tomasi, M. Tristram, M. Tucci, J.-P. Uzan, L. Valenziano, J. Valiviita, B. Van Tent, P. Vielva, F. Villa, L. A. Wade, D. Yvon, A. Zacchei, and A. Zonca. Planck intermediate results. XXIV. Constraints on variations in fundamental constants. *A&A*, 580:A22, Aug. 2015.
69. Planck Collaboration, N. Aghanim, Y. Akrami, M. Ashdown, J. Aumont, C. Baccigalupi, M. Ballardini, A. J. Banday, R. B. Barreiro, N. Bartolo, S. Basak, R. Battye, K. Benabed, J. P. Bernard, M. Bersanelli, P. Bielewicz, J. J. Bock, J. R. Bond, J. Borrill, F. R. Bouchet, F. Boulanger, M. Bucher, C. Burigana, R. C. Butler, E. Calabrese, J. F. Cardoso, J. Carron, A. Challinor, H. C. Chiang, J. Chluba, L. P. L. Colombo, C. Combet, D. Contreras, B. P. Crill, F. Cuttaia, P. de Bernardis, G. de Zotti, J. Delabrouille, J. M. Delouis, E. Di Valentino, J. M. Diego, O. Doré, M. Douspis, A. Ducout, X. Dupac, S. Dusini, G. Efstathiou, F. Elsner, T. A. Enßlin, H. K. Eriksen, Y. Fantaye, M. Farhang, J. Fergusson, R. Fernandez-Cobos, F. Finelli, F. Forastieri, M. Frailis, E. Franceschi, A. Frolov, S. Galeotta, S. Galli, K. Ganga, R. T. Génova-Santos, M. Gerbino, T. Ghosh, J. González-Nuevo, K. M. Górski, S. Gratton, A. Gruppuso, J. E. Gudmundsson, J. Hamann, W. Handley, D. Herranz, E. Hivon, Z. Huang, A. H. Jaffe, W. C. Jones, A. Karakci, E. Keihänen, R. Keskitalo, K. Kiiveri, J. Kim, T. S. Kisner, L. Knox, N. Krachmalnicoff, M. Kunz, H. Kurki-Suonio, G. Lagache, J. M. Lamarre, A. Lasenby, M. Lattanzi, C. R. Lawrence, M. Le Jeune, P. Lemos, J. Lesgourgues, F. Levrier, A. Lewis, M. Liguori, P. B. Lilje, M. Lilley, V. Lindholm, M. López-Caniago, P. M. Lubin, Y. Z. Ma, J. F. Macías-Pérez, G. Maggio, D. Maino, N. Mandolesi, A. Mangilli, A. Marcos-Caballero, M. Maris, P. G. Martin, M. Martinelli, E. Martínez-González, S. Matarrese, N. Mauri, J. D. McEwen, P. R. Meinhold, A. Melchiorri, A. Mennella, M. Migliaccio, M. Millea, S. Mitra, M. A. Miville-Deschênes, D. Molinari, L. Montier, G. Morgante, A. Moss, P. Natoli, H. U. Nørgaard-Nielsen, L. Pagano, D. Paoletti, B. Partridge, G. Patanchon, H. V. Peiris, F. Perrotta, V. Pettorino, F. Piacentini, L. Polastri, G. Polenta, J. L. Puget, J. P. Rachen, M. Reinecke, M. Remazeilles, A. Renzi, G. Rocha, C. Rosset, G. Roudier, J. A. Rubiño-Martín, B. Ruiz-Granados, L. Salvati, M. Sandri, M. Savelainen, D. Scott, E. P. S. Shellard, C. Sirignano, G. Sirri, L. D. Spencer, R. Sunyaev, A. S. Suur-Uski, J. A. Tauber, D. Tavagnacco, M. Tenti, L. Toffolatti, M. Tomasi, T. Trombetti, L. Valenziano, J. Valiviita, B. Van Tent, L. Vibert, P. Vielva, F. Villa, N. Vittorio, B. D. Wandelt, I. K. Wehus, M. White, S. D. M. White, A. Zacchei, and A. Zonca. Planck 2018 results. VI. Cosmological parameters. *ArXiv:1807.06209*, July 2018.
70. Planck Collaboration, N. Aghanim, Y. Akrami, M. Ashdown, J. Aumont, C. Baccigalupi, M. Ballardini, A. J. Banday, R. B. Barreiro, N. Bartolo, S. Basak, K. Benabed, J. P. Bernard,

- M. Bersanelli, P. Bielewicz, J. J. Bock, J. R. Bond, J. Borrill, F. R. Bouchet, F. Boulanger, M. Bucher, C. Burigana, R. C. Butler, E. Calabrese, J. F. Cardoso, J. Carron, B. Casaponsa, A. Challinor, H. C. Chiang, L. P. L. Colombo, C. Combet, B. P. Crill, F. Cuttaia, P. de Bernardis, A. de Rosa, G. de Zotti, J. Delabrouille, J. M. Delouis, E. Di Valentino, J. M. Diego, O. Doré, M. Douspis, A. Ducout, X. Dupac, S. Dusini, G. Efstathiou, F. Elsner, T. A. Enßlin, H. K. Eriksen, Y. Fantaye, R. Fernandez-Cobos, F. Finelli, M. Frailis, A. A. Fraisse, E. Franceschi, A. Frolov, S. Galeotta, S. Galli, K. Ganga, R. T. Génova-Santos, M. Gerbino, T. Ghosh, Y. Giraud-Héraud, J. González-Nuevo, K. M. Górski, S. Gratton, A. Gruppuso, J. E. Gudmundsson, J. Hamann, W. Handley, F. K. Hansen, D. Herranz, E. Hivon, Z. Huang, A. H. Jaffe, W. C. Jones, E. Keihänen, R. Keskitalo, K. Kiiveri, J. Kim, T. S. Kisner, N. Krachmalnicoff, M. Kunz, H. Kurki-Suonio, G. Lagache, J. M. Lamarre, A. Lasenby, M. Lattanzi, C. R. Lawrence, M. Le Jeune, F. Levrier, A. Lewis, M. Liguori, P. B. Lilje, M. Lilley, V. Lindholm, M. López-Caniego, P. M. Lubin, Y. Z. Ma, J. F. Macías-Pérez, G. Maggio, D. Maino, N. Mandolesi, A. Mangilli, A. Marcos-Caballero, M. Maris, P. G. Martin, E. Martínez-González, S. Matarrese, N. Mauri, J. D. McEwen, P. R. Meinhold, A. Melchiorri, A. Mennella, M. Migliaccio, M. Millea, M. A. Miville-Deschênes, D. Molinari, A. Moneti, L. Montier, G. Morgante, A. Moss, P. Natoli, H. U. Nørgaard-Nielsen, L. Pagano, D. Paoletti, B. Partridge, G. Patanchon, H. V. Peiris, F. Perrotta, V. Pettorino, F. Piacentini, G. Polenta, J. L. Puget, J. P. Rachen, M. Reinecke, M. Remazeilles, A. Renzi, G. Rocha, C. Rosset, G. Roudier, J. A. Rubiño-Martín, B. Ruiz-Granados, L. Salvati, M. Sandri, M. Savelainen, D. Scott, E. P. S. Shellard, C. Sirignano, G. Sirri, L. D. Spencer, R. Sunyaev, A. S. Suur-Uski, J. A. Tauber, D. Tavagnacco, M. Tenti, L. Toffolatti, M. Tomasi, T. Trombetti, J. Valiviita, B. Van Tent, P. Vielva, F. Villa, N. Vittorio, B. D. Wandelt, I. K. Wehus, A. Zacchei, and A. Zonca. Planck 2018 results. V. CMB power spectra and likelihoods. *arXiv e-prints*, page arXiv:1907.12875, Jul 2019.
71. Planck Collaboration, N. Aghanim, Y. Akrami, M. Ashdown, J. Aumont, C. Baccigalupi, M. Ballardini, A. J. Banday, R. B. Barreiro, N. Bartolo, S. Basak, K. Benabed, J. P. Bernard, M. Bersanelli, P. Bielewicz, J. J. Bock, J. R. Bond, J. Borrill, F. R. Bouchet, F. Boulanger, M. Bucher, C. Burigana, E. Calabrese, J. F. Cardoso, J. Carron, A. Challinor, H. C. Chiang, L. P. L. Colombo, C. Combet, B. P. Crill, F. Cuttaia, P. de Bernardis, G. de Zotti, J. Delabrouille, E. Di Valentino, J. M. Diego, O. Doré, M. Douspis, A. Ducout, X. Dupac, G. Efstathiou, F. Elsner, T. A. Enßlin, H. K. Eriksen, Y. Fantaye, R. Fernandez-Cobos, F. Forastieri, M. Frailis, A. A. Fraisse, E. Franceschi, A. Frolov, S. Galeotta, S. Galli, K. Ganga, R. T. Génova-Santos, M. Gerbino, T. Ghosh, J. González-Nuevo, K. M. Górski, S. Gratton, A. Gruppuso, J. E. Gudmundsson, J. Hamann, W. Handley, F. K. Hansen, D. Herranz, E. Hivon, Z. Huang, A. H. Jaffe, W. C. Jones, A. Karakci, E. Keihänen, R. Keskitalo, K. Kiiveri, J. Kim, L. Knox, N. Krachmalnicoff, M. Kunz, H. Kurki-Suonio, G. Lagache, J. M. Lamarre, A. Lasenby, M. Lattanzi, C. R. Lawrence, M. Le Jeune, F. Levrier, A. Lewis, M. Liguori, P. B. Lilje, V. Lindholm, M. López-Caniego, P. M. Lubin, Y. Z. Ma, J. F. Macías-Pérez, G. Maggio, D. Maino, N. Mandolesi, A. Mangilli, A. Marcos-Caballero, M. Maris, P. G. Martin, E. Martínez-González, S. Matarrese, N. Mauri, J. D. McEwen, A. Melchiorri, A. Mennella, M. Migliaccio, M. A. Miville-Deschênes, D. Molinari, A. Moneti, L. Montier, G. Morgante, A. Moss, P. Natoli, L. Pagano, D. Paoletti, B. Partridge, G. Patanchon, F. Perrotta, V. Pettorino, F. Piacentini, L. Polastri, G. Polenta, J. L. Puget, J. P. Rachen, M. Reinecke, M. Remazeilles, A. Renzi, G. Rocha, C. Rosset, G. Roudier, J. A. Rubiño-Martín, B. Ruiz-Granados, L. Salvati, M. Sandri, M. Savelainen, D. Scott, C. Sirignano, R. Sunyaev, A. S. Suur-Uski, J. A. Tauber, D. Tavagnacco, M. Tenti, L. Toffolatti, M. Tomasi, T. Trombetti, J. Valiviita, B. Van Tent, P. Vielva, F. Villa, N. Vittorio, B. D. Wandelt, I. K. Wehus, M. White, S. D. M. White, A. Zacchei, and A. Zonca. Planck 2018 results. VIII. Gravitational lensing. *arXiv e-prints*, page arXiv:1807.06210, Jul 2018.
72. V. Poulin, T. L. Smith, and T. Karwal. The Ups and Downs of Early Dark Energy solutions to the Hubble tension: a review of models, hints and constraints circa 2023. *arXiv e-prints*, page arXiv:2302.09032, Feb. 2023.

73. M. Raveri. Resolving the Hubble tension at late times with Dark Energy. *arXiv e-prints*, page arXiv:2309.06795, Sept. 2023.
74. A. G. Riess, S. Casertano, W. Yuan, L. M. Macri, and D. Scolnic. Large Magellanic Cloud Cepheid Standards Provide a 1% Foundation for the Determination of the Hubble Constant and Stronger Evidence for Physics beyond Λ CDM. *Astrophys. J.*, 876(1):85, 2019.
75. G. Rocha, R. Trotta, C. J. A. P. Martins, A. Melchiorri, P. P. Avelino, R. Bean, and P. T. P. Viana. Measuring α in the early Universe: cosmic microwave background polarization, reionization and the Fisher matrix analysis. *MNRAS*, 352:20–38, July 2004.
76. T. Rosenband, D. B. Hume, P. O. Schmidt, C. W. Chou, A. Brusch, L. Lorini, W. H. Oskay, R. E. Drullinger, T. M. Fortier, J. E. Stalnaker, S. A. Diddams, W. C. Swann, N. R. Newbury, W. M. Itano, D. J. Wineland, and J. C. Bergquist. Frequency ratio of al^+ and hg^+ single-ion optical clocks; metrology at the 17th decimal place. *Science*, 319(5871):1808–1812, 2008.
77. J. A. Rubiño-Martín, J. Chluba, W. A. Fendt, and B. D. Wandelt. Estimating the impact of recombination uncertainties on the cosmological parameter constraints from cosmic microwave background experiments. *MNRAS*, 403:439–452, Mar. 2010.
78. J. A. Rubiño-Martín, J. Chluba, and R. A. Sunyaev. Lines in the cosmic microwave background spectrum from the epoch of cosmological helium recombination. *A&A*, 485:377–393, July 2008.
79. J. A. Rubiño-Martín, C. Hernández-Monteagudo, and R. A. Sunyaev. The imprint of cosmological hydrogen recombination lines on the power spectrum of the CMB. *A&A*, 438:461–473, Aug. 2005.
80. G. B. Rybicki and I. P. dell’Antonio. The time development of a resonance line in the expanding universe. *ApJ*, 427:603–617, June 1994.
81. M. Sathyanarayana Rao, R. Subrahmanyam, N. Udaya Shankar, and J. Chluba. On the Detection of Spectral Ripples from the Recombination Epoch. *ApJ*, 810:3, Sept. 2015.
82. N. Schöneberg, G. F. Abellán, A. P. Sánchez, S. J. Witte, V. Poulin, and J. Lesgourgues. The H_0 Olympics: A fair ranking of proposed models. *Phys.Rep.*, 984:1–55, Oct. 2022.
83. C. G. Scóccola, S. J. Landau, and H. Vucetich. WMAP 5-year constraints on time variation of α and m_e . *Memorie della Societ Astronomica Italiana*, 80:814–+, 2009.
84. S. Seager, D. D. Sasselov, and D. Scott. A New Calculation of the Recombination Epoch. *ApJL*, 523:L1–L5, Sept. 1999.
85. S. Seager, D. D. Sasselov, and D. Scott. How Exactly Did the Universe Become Neutral? *ApJS*, 128:407–430, June 2000.
86. T. Sekiguchi and T. Takahashi. Early recombination as a solution to the H_0 tension. *Phys.Rev.D*, 103(8):083507, Apr. 2021.
87. J. R. Shaw and J. Chluba. Precise cosmological parameter estimation using COSMOREC. *MNRAS*, 415:1343–1354, Aug. 2011.
88. L. D. Shaw, D. Nagai, S. Bhattacharya, and E. T. Lau. Impact of Cluster Physics on the Sunyaev-Zel’dovich Power Spectrum. *ApJ*, 725:1452–1465, Dec. 2010.
89. T. L. Smith, D. Grin, D. Robinson, and D. Qi. Probing spatial variation of the fine-structure constant using the CMB. *Phys.Rev.D*, 99(4):043531, Feb. 2019.
90. V. V. Sobolev. *Moving envelopes of stars*. Cambridge: Harvard University Press, 1960, 1960.
91. R. A. Sunyaev and J. Chluba. Signals from the epoch of cosmological recombination (Karl Schwarzschild Award Lecture 2008). *Astronomische Nachrichten*, 330:657–+, 2009.
92. R. A. Sunyaev and Y. B. Zeldovich. Small-Scale Fluctuations of Relic Radiation. *ApSS*, 7:3–+, 1970.
93. H. Tohfa, J. Crump, E. Baker, L. Hart, D. Grin, M. Brosius, and J. Chluba. A cosmic microwave background search for fine-structure constant evolution. *arXiv e-prints*, page arXiv:2307.06768, July 2023.
94. J.-P. Uzan. The fundamental constants and their variation: observational and theoretical status. *Reviews of Modern Physics*, 75:403–455, Apr. 2003.
95. J.-P. Uzan. Varying Constants, Gravitation and Cosmology. *Living Reviews in Relativity*, 14:2, Mar. 2011.
96. W. Y. Wong, A. Moss, and D. Scott. How well do we understand cosmological recombination? *MNRAS*, 386:1023–1028, May 2008.

97. Y. B. Zeldovich, V. G. Kurt, and R. A. Syunyaev. Recombination of Hydrogen in the Hot Model of the Universe. *Zhurnal Eksperimental noi i Teoreticheskoi Fiziki*, 55:278–286, July 1968.